The Band Model and the Etching Mechanism of Silicon in Aqueous KOH

Lai-Cheng Chen, Minjan Chen, Chenhsin Lien,[a] and Chi-Chao Wan

Department of Chemical Engineering, [a]Department of Electrical Engineering, National Tsing Hua University, Hsinchu 300, Taiwan

ABSTRACT

The energy band diagram of n-Si in aqueous 2*M* KOH is constructed by the measured open-circuit potential and the flatband voltage. A photocurrent susceptivity method was proposed to determine the flatband voltage. A flatband voltage of −1.04 V/SCE (saturated calomel electrode) for the n-Si in 2*M* KOH was determined by this new method. The energy band diagram of the p-Si in the same electrolyte is also constructed. Accumulation of carriers at the n-Si/KOH interface is predicted by the band diagram and confirmed by the ohmic-contact-like I-V curve. Depletion of carriers at p-Si/KOH interface is predicted by the band diagram and confirmed by the rectifying I-V characteristics. The passivation of Si under anodic bias is attributed to the formation of an oxide film. The competition between the oxidation rate and the diffusion rate of oxidation product determines whether the anodic oxidation is an etching or passivation process. The etching oxidation is assumed to be dominated by the electrochemical reaction. The transport of these carriers which participate in the electrochemical reaction can be explained by the energy band diagram. All etching or passivation phenomena are consistent with the prediction from the band diagram viewpoint. The etch stop for heavily doped Si is attributed to the enhanced growth rate of oxide film under high carrier concentration.

The energy band diagram of the semiconductor electrode is a useful tool for understanding transport phenomena of the carriers in the electrochemical reaction, such as electrodeposition or electroless deposition of metal onto semiconductor; selective etching and decomposition of the semiconductor electrode.[1-5] To construct the energy band diagram of Si in aqueous KOH, which is involved in the anisotropic etching reaction, is useful in understanding the carrier-transport phenomena as well as the etching mechanism.

The anisotropic etching of Si in the alkaline electrolyte has long been recognized and employed in the fabrication of microstructures such as diaphragms,[6-8] cantilever beams,[9] grooves,[10] etc. These microstructures are important in the manufacture of microsensors and microactuators which can be integrated in a single chip. The widespread application of the anisotropic etching techniques calls for the construction of the quantitative energy band diagram of Si in the alkaline electrolyte to describe the transport of carriers during etching. Palik *et al.*,[11,12] and Ozdemir and Smith[13] qualitatively explained the I-V behaviors of Si in KOH by using a simple qualitative energy band diagram. Seidel *et al.*[14] constructed the energy band diagram of Si in the alkaline electrolyte by aligning the Fermi level between the Si and the electrolyte. They attributed the Fermi level of electrolyte (H_2O/OH^-) to be 0.8 V/NHE (normal hydrogen electrode) which is the standard redox potential modified by the Nernst equation. Sundaram and Chang also constructed the energy band diagram of Si in hydrazine to give a qualitative explanation of the different I-V behaviors for n- and p-type Si by the same method.[15] Alternatively, the Fermi level of the electrolyte can be determined by measuring the open-circuit potential (OCP) with respect to a reference electrode (for example, NHE) of which the Fermi level is fixed and used as a reference.[11]

In this article, the quantitative energy band diagram of n-Si in aqueous KOH was constructed from the measured OCP and the flatband voltage. The energy band diagram of p-Si in the same electrolyte also was constructed. The measurement of I-V characteristics are performed to verify these energy band diagrams. Accumulation of carriers at the n-Si/KOH interface is predicted by the band diagram and confirmed by the ohmic-contactlike I-V curve. Depletion of carriers at the p-Si/KOH interface is predicted by the band diagram and confirmed by the rectifying I-V characteristics. The passivation for Si under anodic bias is attributed to the formation of an oxide film. The competition between the oxidation rate and the diffusion rate of oxidized product determines whether the anodic oxidation is an etching or passivating process. The carriers needed in the electrochemical reaction are explained by the energy band diagram. All observed etching or passivating phenomena are consistent with the energy band diagram. The etch stop for heavily doped Si is studied and attributed to the enhanced growth rate of oxide film under high carrier concentration.

Experimental

Commercial n- and p-Si with (100) orientation were used. The resistivity of n-Si was 6 to 11 Ω-cm, and that of p-Si was 15 to 20 Ω-cm. These samples were degreased successively in boiling trichloroethane, acetone, and methanol. After rinsing with deionized water, the samples were dipped in HF/H_2O solution to remove the native oxide. In-Ga eutectic alloy was pasted between the sample and a copper plate to provide good contact for electrochemical measurements. The sample and copper plate were fixed in a Teflon sample holder where the exposed area of Si was 0.072 cm^2. Before immersion in the 2*M* KOH solution, the sample was dipped in HF/H_2O solution for several minutes, and then rinsed with deionized water.

A conventional three-electrode cell with a Pt counter-electrode and a saturated calomel electrode (SCE) was used. After immersing the sample in the KOH solution, the OCP was recorded with time. The steady value (after ~30 min) was defined as the OCP of the electrochemical system at equilibrium. Potentiodynamic method with a sweep rate of 5 mV/s was used to measure the I-V curves. The I-V curves were made under illumination with a Philips' tungsten lamp, 60 W, positioned 10 cm from the sample.

Photocurrent susceptivity method.—A new photocurrent susceptivity method was used to find the flatband voltage of n-Si in KOH. After the sample reached equilibrium, the potential of the n-Si was controlled at slightly more anodic potential than the OCP by the potentiostat (RDE 4, Pine Instrument Co.). The steady current was recorded, referred to as the dark current, then the light was turned on, and the anodic current changed abruptly and reached a steady value which was referred to as the photocurrent. The photocurrent susceptivity (ΔI) is defined as the difference between the photocurrent and the dark current. The specific voltage which makes the photocurrent susceptivity zero is defined as the flatband voltage. The increase in the anodic current of n-Si under illumination comes from the contribution of photogenerated holes. There exists an electric field which separates the photogenerated electrons and holes in the n-Si as the energy band bends. The contribution of these photogenerated holes to the anodic current is the photocurrent susceptivity (ΔI). Since this electric field decreases as anodic bias is applied

to the n-Si, the opportunity for recombination of the photogenerated electrons and holes is enhanced. Consequently, the photocurrent susceptivity decreases when the applied anodic bias is close to the flatband voltage. At the flatband voltage, the photocurrent susceptivity should be zero due to disappearance of the electric field.

Results

Open-circuit potential.—The OCP of n- and p-Si in 2*M* KOH was measured to be −1.25 and −0.95 V, respectively. These values are close to the results obtained by Palik *et al.*[16] and Glembocki and Stahlbush.[17] The OCP shifted anodically from −0.95 to −0.75 V for p-Si in 2*M* KOH under illumination, and no apparent shift of OCP was observed for n-Si under illumination. These OCP shifts are consistent with results reported by Ozdemir and Smith.[13]

I-V curves of n- and p-Si in 2M KOH.—Figure 1 shows the I-V curves of n- and p-Si in the KOH electrolyte under normal room light. No apparent change of I-V curves was observed for the system in the dark. The passivation peak was similar in magnitude for both n- and p-Si. The corresponding potentials of the passivation peak are −0.92 and −0.71 V in n- and p-Si, respectively. The passivation peak is rounded for the n-Si while sharp for the p-Si. Beyond the passivation peak, the anodic current of the n-Si increases slightly from 2.3 to 10 V. For the p-Si, a large increase in anodic current and two additional peaks located at 3.7 and 8.7 V are observed. Under the cathodic bias, the cathodic current increases almost linearly with cathodic bias for the n-Si, while it saturates at ~25 μA/cm² for the p-Si. The inset in Fig. 1 gives a detailed view of I-V curves near the OCP. Before the passivation peak, the I-V characteristics show a linear ohmic-contact-like behavior for n-Si/KOH and a rectifying Schottky-contact-like behavior for p-Si/KOH.

The effect of illumination on the I-V curve is shown in Fig. 2 and 3 for n-Si and p-Si, respectively. There is significant change in the I-V curve under illumination for the anodic current of the n-Si, and the cathodic current of the p-Si. For the n-Si, the anodic current beyond the passivation potential (PP) at −0.92 V increases and two peaks appear at 3.7 and 8.7 V under illumination. The anodic current of the n-Si under illumination behaves the same way as the anodic current of the p-Si in the dark. For p-Si under illumination, the cathodic current does not saturate and increase with the cathodic bias.

Flatband voltage.—By means of the photocurrent susceptivity method, the flatband voltage of the n-Si in 2*M* KOH was measured to be −1.04 V as shown in Fig. 4. This

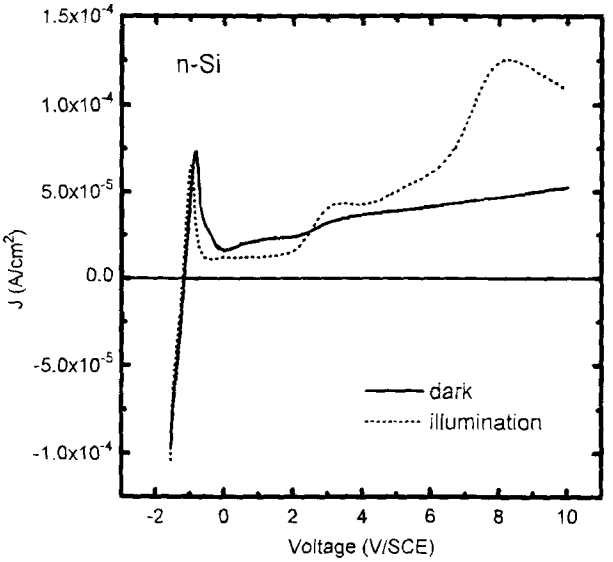

Fig. 2. The comparison of the I-V curves of n-Si in 2M KOH in the dark and illumination.

value agrees well with the result of Glembocki and Stahlbush who determined the flatband voltage by the electrofluence and the capacitance measurements.[17] This value is also consistent with the flatband voltage of the n-Si(111) in 2*M* NaOH obtained by photocurrent measurement with weak modulated illumination using a lock-in amplifier.[18] As the anodic bias is less than the flatband voltage, the energy band bends downward and the silicon is in accumulation phase. There are many electrons in the surface of silicon and the recombination probability for holes is high. Still a steady-state excess hole concentration is reached, thus some photogenerated electron-hole pair is separated by the electric field and a small and nearly constant photocurrent susceptivity results. Since this electric field decreases as anodic bias is applied to the n-Si, the opportunity for recombination of the photogenerated electrons and holes is enhanced. Consequently, the photocurrent susceptivity decreases when the applied anodic bias is closest to the flatband voltage. At the flatband voltage, the photocurrent susceptivity should be zero due to disappearance of the electric field. As the anodic bias is increased further beyond flatband voltage, the energy band bends upward and a depletion region is formed. Most of the pho-

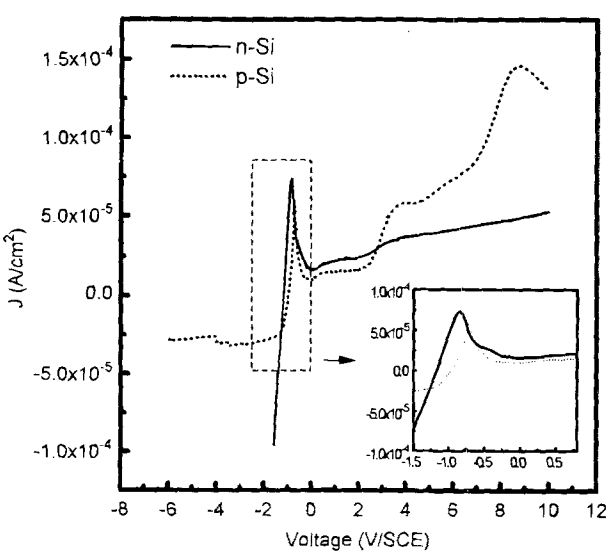

Fig. 1. The I-V characteristics for both n- and p-Si contact to 2M KOH in the dark. The inset is expansion of the curves near the OCP.

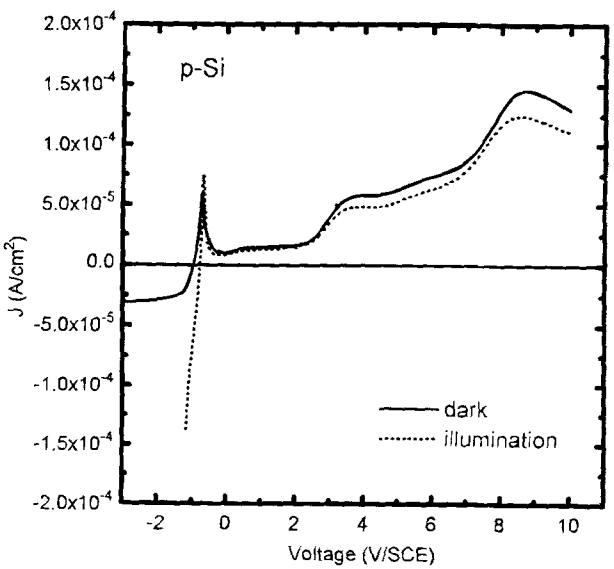

Fig. 3. The comparison of the I-V curves of p-Si in 2M KOH in the dark and illumination.

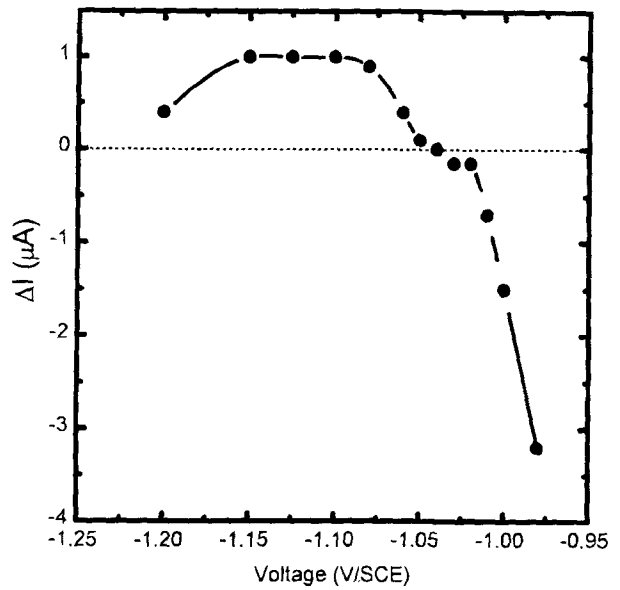

Fig. 4. The anodic photocurrent susceptivity in n-Si as a function of the applied bias. The flatband voltage is −1.04 V/SCE.

togenerated electron-hole pairs inside this depletion region can be separated and can contribute to the photocurrent susceptivity. Since the width of depletion region widens as the bias is increased, the photocurrent susceptivity increases with the anodic bias.

The photocurrent susceptivity method cannot be used to measure the flatband voltage of the p-Si in 2*M* KOH because (*i*) the anodic photocurrent susceptivity is too weak to be detected and (*ii*) the flatband voltage of p-Si is more anodic than the passivation potential. Hence the surface of the p-Si is passivated before the anodic bias reaches the flatband voltage.

Discussion

The energy band diagram of n- and p-Si in 2M KOH.—n-Si/KOH.—The energy band of n-Si bends in contact with aqueous KOH. Such energy band bending comes from the alignment of the Fermi level between the n-Si and the electrolyte. The Fermi level of the electrolyte is defined as the redox potential of the redox couple which is involved in the etching reaction. The redox couple involved in the etching reaction of Si in the alkaline electrolyte is OH^-/H_2O.[11,14] The redox potential of OH^-/H_2O may not necessarily be located at its standard position due to the activity of ions. Thus the Fermi level of OH^-/H_2O varies in different alkaline electrolytes. The OCP of n-Si in KOH is different from that in other alkaline electrolytes. Therefore, the Fermi level of OH^-/H_2O in 2*M* KOH should be different from other alkaline electrolyte such as ammonia. Seidel *et al.*[14] and Sundaram and Chang[15] chose the Nernst equation to adjust the standard redox potential of OH^-/H_2O by −59 mV/pH for the calculation of Fermi level for the electrolyte. Based on our findings for the different alkaline electrolytes, this method seems questionable. In this article, the Fermi level of the electrolyte which is aligned with the Fermi level of the semiconductor at equilibrium is obtained by measuring the OCP of the semiconductor electrode in the electrolyte.[11]

To construct the energy band diagram of the semiconductor, the location of the conduction bandedge at the interface (E_{cs}), that is the built-in voltage of the semiconductor, should be determined, too. This E_{cs} can be determined from the measurement of the flatband voltage. At the flatband voltage, the energy band bending disappears and E_{cs} is located above the Fermi level by $q\Phi_t$. The magnitude of $q\Phi_t$ can be calculated from the doping concentration. The potential drop across the Helmholtz double layer can be estimated from the absorbed charges density. Morrison[19] has estimated that the potential drop for 10^{16} charge/m^2 absorbed on metal or insulator surface is only ~0.016 V. Therefore, we assume that most of the potential drop at equilibrium falls on the semiconductor, the energy band bending for the n-Si at equilibrium can be determined from the knowledge of the OCP and the flatband bias voltage.

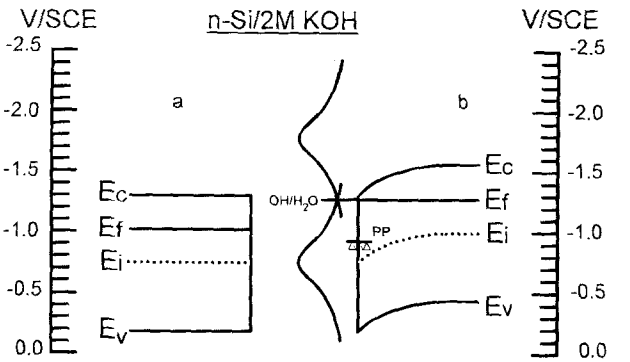

Fig. 5. The energy band diagram of n-Si contacts to 2*M* KOH (a) at the flatband bias and (b) at equilibrium. The scale shown is referred to the SCE. The triangle indicates the position of the passivation potential (PP).

Energy band diagrams for n-Si in 2*M* KOH at equilibrium and at flatband bias are illustrated in Fig. 5. From the measured flatband voltage −1.04 V, and the OCP, −1.25 V, at equilibrium, the energy band of the n-Si bends 0.21 eV downward at the interface (Fig. 5b). Thus, the surface of n-Si is accumulated with electrons. This accumulation of majority carriers leads to the formation of ohmic contact between n-Si and KOH.

p-Si/KOH.—Since the electron affinity χ should be the same for both n-Si and p-Si in the same electrolyte, the energy band diagram of the p-Si in 2*M* KOH can be constructed by measuring the OCP without any knowledge of the flatband voltage. The energy band diagram of p-Si in 2*M* KOH at equilibrium together with flatband bias are shown in Fig. 6. A flatband voltage of −0.44 V is obtained. At equilibrium, the energy band of the p-Si in KOH bends downward by 0.49 eV, which means a potential barrier near the interface is formed. The magnitude of energy band bending ϕ_S in Fig. 6b is less than $2\phi_f$. This shows that the surface of p-Si is not yet in strong inversion. Characteristic potentials are summarized in Table I.

The I-V Characteristics

The I-V characteristics before passivation.—With the aid of energy band diagrams, the difference between I-V characteristics of n-Si and p-Si in 2*M* KOH can be explained. By ignoring the occurrence of the passivation at the anodic bias, (passivation changes the structure from Si/electrolyte to Si/oxide/electrolyte) the transport of free carriers and

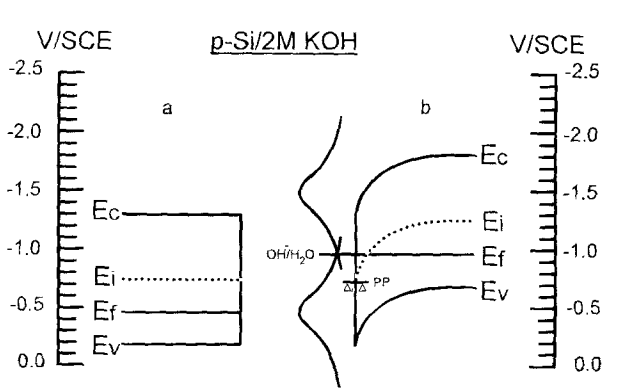

Fig. 6. The energy band diagram of p-Si contacts to 2*M* KOH (a) at the flatband bias and (b) at equilibrium.

Table I. Characteristic potentials for n- and p-Si in aqueous 2M KOH.

	OCP (V/SCE)	V_{FB} (V/SCE)	PP (V/SCE)	PP-OCP (V)	ϕ_S (V)	ϕ_f (V)
n-Si	−1.25	−1.04	−0.92	0.33	0.21	0.28
p-Si	−0.95	−0.44	−0.71	0.24	0.49	0.30

the corresponding energy band bending with various bias are plotted schematically in Fig. 7 and 8.

n-Si/KOH.—With cathodic bias, as shown in Fig. 7a, electrons flow freely from the silicon through the ohmic-like junction of n-Si/electrolyte and drift across the thin Helmholtz double layer to the electrolyte. These electrons participate in the following cathodic reaction

$$2H_2O + 2e^- \rightarrow H_2 + 2\ OH^- \quad [1]$$

With anodic bias, electrons flow from the electrolyte to n-Si, and an anodic reaction occurs raising the Si to a higher oxidation state. It is clear from Fig. 8a, b that there is no potential barrier to restrict the transport of electrons across the n-Si/electrolyte interface with either the cathodic bias or the anodic bias. Thus, the current increases linearly with both the cathodic bias and the anodic bias for the n-Si/KOH (Fig. 7, solid). This linear I-V relation can be clearly observed near the OCP bias as shown in the inset in

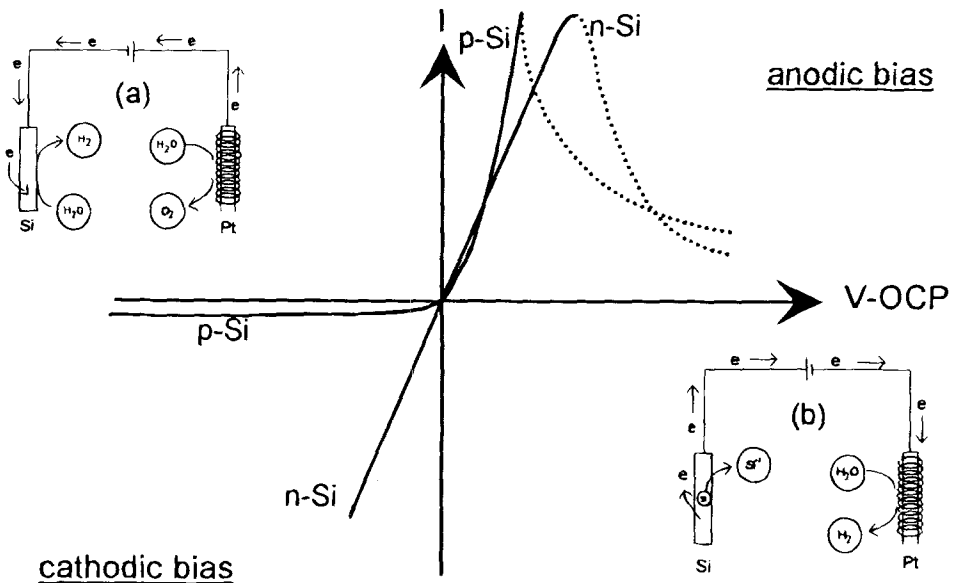

Fig. 7. The transportation of electrons as well as the predicted I-V characteristics for n-Si and p-Si under (a) cathodic and (b) anodic bias.

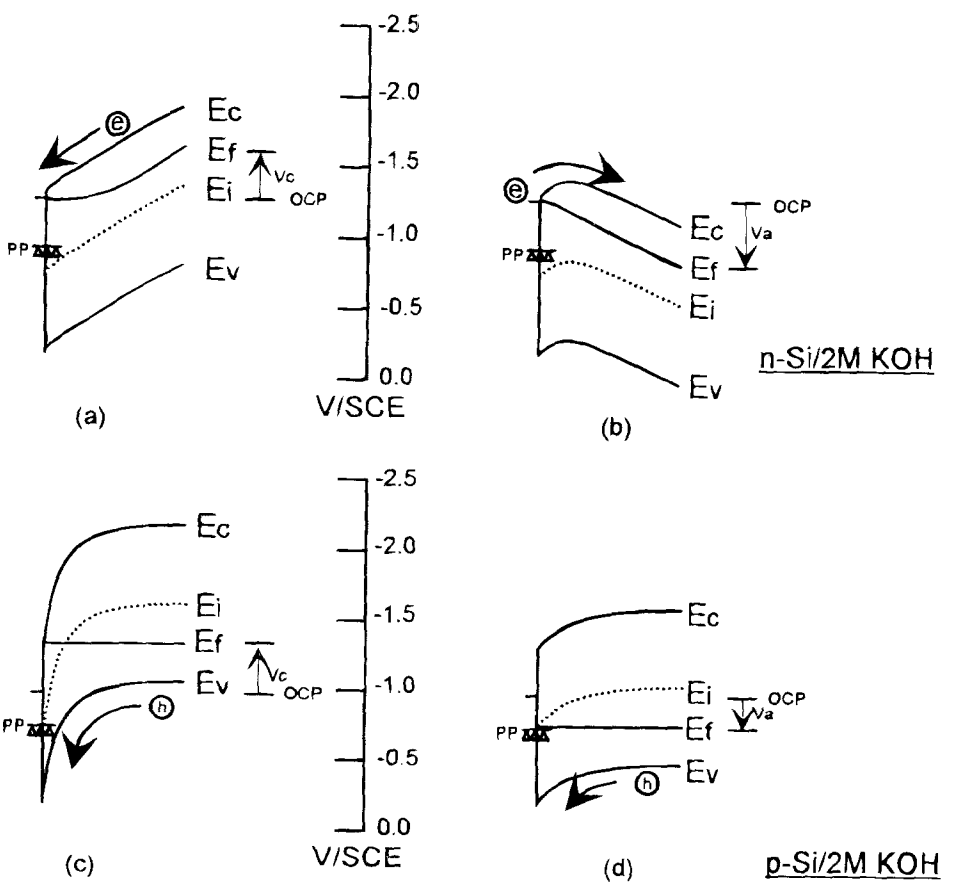

Fig. 8. The energy band diagrams and corresponding carrier-transport diagram for n-Si and p-Si under cathodic bias (a, c) and anodic bias (b, d).

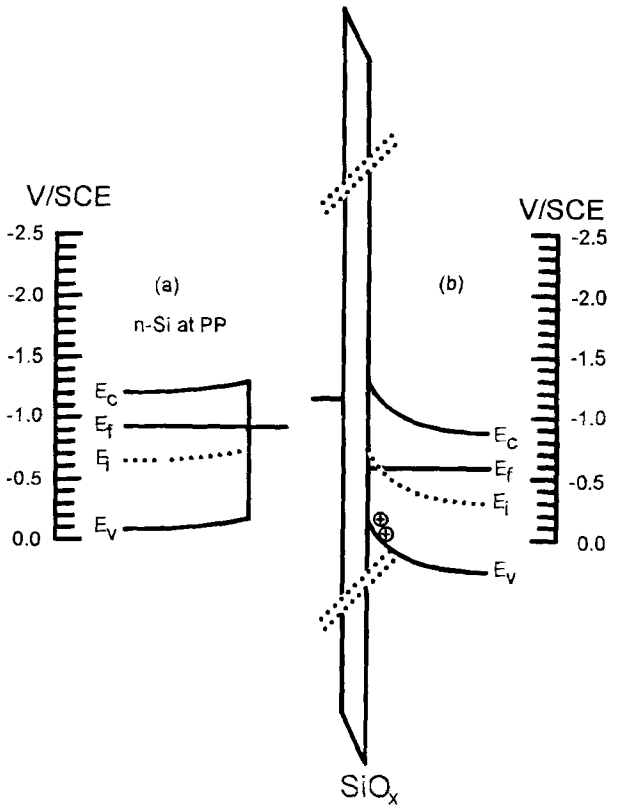

Fig. 9. The energy band diagrams of n-Si biased at the PP (a) before and (b) after the formation of oxide film.

Fig. 1. A completely different I-V characteristic was observed for n-Ge in the alkaline solution.[20] The anodic current for the n-Ge/KOH system was found saturate at a small leakage current. Based on this measured I-V behavior for the n-Ge electrode in the alkaline electrolyte, Faust and Palik[21] and Palik *et al.*[11,12] predicted that the anodic current of the n-Si in KOH should also saturate at a small leakage current. However, it is clear from Fig. 1 that the anodic current does not saturate with anodic bias. This observation is consistent with the energy band diagram of the n-Si in KOH constructed in this article.

p-Si/KOH.—The I-V characteristics of the p-Si in 2*M* KOH can be explained by the energy band diagram constructed in Fig. 6. There is a potential energy barrier formed at the p-Si/KOH interface. This barrier restricts the current flow in the anodic direction only. With cathodic bias, only a minute amount of leakage current flows. The measured I-V behavior shows a small leakage with cathodic bias and a steep rise of current with anodic bias. This observation again is consistent with the prediction from the energy band diagram. The anodic current rises exponentially with the anodic bias until an oxide film forms on the surface of the p-Si which decreases the anodic current. The sharpness of the passivation peak is a result of this sharp exponential rise of anodic current. The relative dullness of the passivation peak for the n-Si is the consequence of the slow linear rise of anodic current.

The I-V characteristics beyond passivation.—It is well known that the anodic current decreases abruptly due to the formation of an oxide film at the surface of Si in KOH under an anodic bias level beyond the PP. The composition of the anodically formed oxide film was determined as SiO_x ($0 \leq x \leq 2$) by optical measurement.[22] Although the anodic oxide film is less dense than thermal oxide film, it is still a good barrier to block carriers. Formation of the oxide film changes the structure from Si/electrolyte to Si/SiO_x/electrolyte. The band diagram for n-Si biased at PP before the oxide formation is shown in Fig. 9a and for n-Si biased beyond the PP after the formation of SiO_x film in Fig. 9b. The corresponding band diagrams for p-Si are plotted in Fig. 10. Since the thickness of SiO_x and the band offset between SiO_x and Si is uncertain, only qualitative band diagrams can be plotted in Fig. 9b and 10b. The energy band bends upward for both n- and p-Si with anodic bias greater than PP. The surface of the n-Si changes from electrons accumulation at equilibrium to depletion as the anodic bias rises and reaches inversion as a layer of holes is formed at the SiO_x/Si interface. The surface of the p-Si remains at hole accumulation as the anodic bias rises becoming degenerate at large biases. The formation of a hole accumulation layer in p-Si and a hole inversion layer in n-Si are consistent with the following electrochemical reaction for oxide film formation[12]

$$\text{-Si-Si-} + OH^- + h^+ \rightarrow \text{-Si-O-Si-} + 1/2\ H_2 \qquad [4]$$

Faust and Palik[21] found that the oxide film grew more by increasing the anodic bias to 10 V. This suggests that the anodic current of both n- and p-Si under anodic bias beyond the passivation is due to electrochemical formation of the oxide film and is related to the concentration of holes at the interface. Therefore, a larger anodic current is expected for the p-Si.

There are two additional peaks located in the I-V curve of the p-Si at 3.7 and 8.7 V. These peaks are observed in the n-Si under illumination. These two peaks are thought to be due to the tunneling of holes through the oxide film. As the anodic bias is high enough, the tunneling of holes through oxide film becomes significant. This enhances the growth rate of the oxide film and decreases the hole tunneling current. Since there is a lack of holes in n-Si unless under illumination, these two peaks cannot be observed for n-Si in dark (as shown in Fig. 2). In addition, the difference between the first peak and the PP is 4 V and the growth rate of oxide formation changes from 6.8 to 41.7 Å/V.[21] Both observations are consistent with the hole tunneling mechanism.

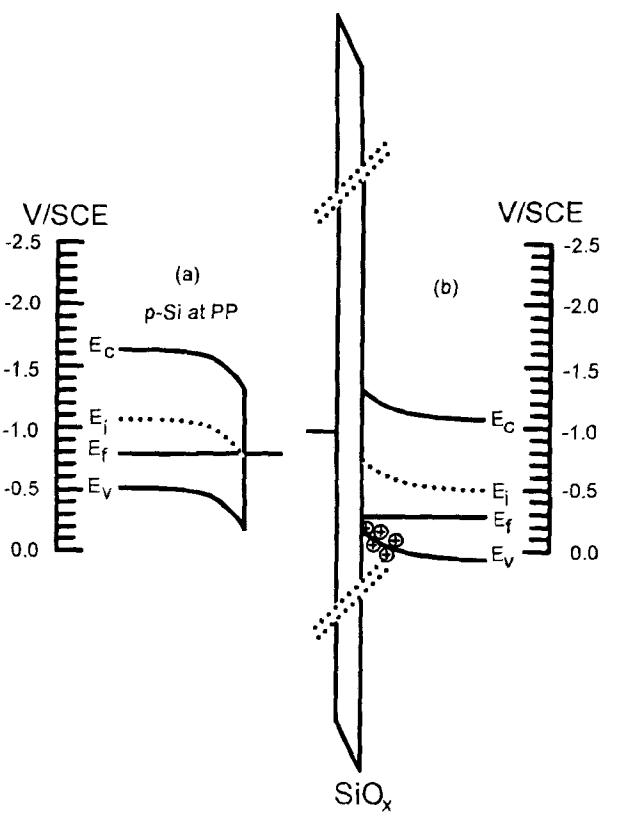

Fig. 10. The energy band diagrams of p-Si biased at the PP (a) before and (b) after the formation of oxide film. The holes accumulate at the interface of Si/SiO_x under anodic bias.

Illumination Effects

Effect of illumination on the OCP.—The change of OCP under illumination for n-Si is different from that for p-Si. There is only a small change of OCP for the n-Si under illumination. However, there is a clear shift of OCP in the anodic direction for the p-Si under illumination. The energy band bends downward near the interface for both n-Si and p-Si, as shown in Fig. 5b and 6b. For the p-Si, there exists a potential barrier and a depletion region near the interface. For the n-Si, there is an accumulation layer at the interface. Thus, for the p-Si, the photogenerated carriers inside the depletion region can be separated by the internal built-in electric field with little recombination and the quasi-Fermi level is split. The OCP for p-Si then shifts in the anodic direction under illumination due to the reduced band bending. As for the n-Si, the photogenerated electron-hole pairs recombine again inside the accumulation region due to the presence of a great number of electrons inside this region. Thus the OCP for n-Si should have little change under illumination.

Effect of illumination on I-V.—It is clear from Fig. 2 and 3 that the obvious changes of the I-V curve under illumination are the anodic current for the n-Si and the cathodic current for the p-Si. These changes can also be understood through energy band diagrams. Since there is no barrier to restrict the current flow in both the anodic and cathodic directions for the n-Si/KOH contact, little changes of the I-V curve for the n-Si under illumination should be expected. This prediction is further confirmed experimentally by the measured I-V curve before passivation potential as shown in Fig. 2. The structure changes from n-Si/electrolyte to n-Si/oxide/electrolyte due to the formation of the oxide film after passivation occurs. This formation of an oxide barrier and further increase of the anodic bias accumulates photogenerated holes at the oxide/Si interface under illumination. These photogenerated holes contribute to the anodic current in the same way as the accumulation of holes for the p-Si in the dark.

For the p-Si contact to a KOH electrolyte, there is only a saturated leakage current flowing under cathodic bias in the dark. The high photogeneration rate splits the quasi-Fermi levels of the silicon/KOH and lowers the Fermi level of p-Si. This lowering of the Fermi level of the p-Si reduces the built-in potential and, eventually, the potential barrier disappears. Without the potential barrier, the cathodic current increases linearly with cathodic bias under illumination.

The Etch Mechanism of Si in KOH

There are several existing models dealing with Si etching in KOH and other alkaline electrolytes at OCP or an applied bias. Raley *et al.*[23] and Seidel *et al.*[14] found the electrochemical reactions dominate in the etching reaction. Glembocki and Stahlbush[17] proposed that both chemical and electrochemical reactions can coexist in the rate-determining step for the etching reaction. Hence, although the role of the chemical reaction is still uncertain, it is clear that the electrochemical reaction plays an important role in the etching reaction. By using the energy band diagram, the transport of carriers during the electrochemical reaction can be understood and the etch stop mechanism becomes clear.

Etching and passivation.—Both etching and passivation of the Si in the alkaline electrolyte are the result of Si oxidation. The competition between the oxidation rate and the diffusion rate of oxidation products to the electrolyte determines whether the anodic oxidation is an etching or passivating process. There exists a critical oxidation rate to build up an oxide film at the surface of the Si. If the oxidation rate is smaller than the critical rate, the oxidation products have sufficient time to diffuse into the electrolyte, and the etching process occurs. However, if the oxidation rate is greater than the critical rate, there is not enough time for the oxidized products to diffuse into the electrolyte, and an oxide film is built up at the surface of the Si and passivation occurs.[22] As a consequence, the passivation is due to the oxide formation rather than breaking of the electron sequence for the reduction oxidation cycle by holes.[24] In addition, the shift of passivation potential to cathodic direction under illumination can be understood as the enhancement of oxide film formation rate due to photogenerated holes.

Etching at the OCP.—Electrochemical etching occurs even at the OCP.[12] Allongue *et al.*[25] proposed that the electrochemical oxidation contributes only a small fraction of the net oxidation rate at the OCP. However, Palik *et al.*[12] show that two H_2 molecules evolve per Si atom etched by measuring the amount of hydrogen evolution during the etching of Si in aqueous KOH. These $2H_2$ molecules should be liberated by either the reduction of H_2O or OH^- and four electrons must be consumed in the reaction. Thus, to treat the etching of Si at OCP as purely a chemical reaction with no electrochemical reaction involved is inappropriate. Therefore, the electrochemical reaction model proposed by Seidel *et al.*[14] is adopted in this article. In this model, an Si atom with dangling bonds is attacked by OH^- to liberate two electrons as follows

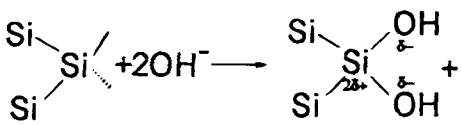

[5]

As indicated in the equilibrium energy band diagram of Si (Fig. 5b and 6b), there is no restriction of electrons flowing from both n-Si and p-Si to the electrolyte. It is well known that the -OH is an electron withdrawing group which weakens the back Si-Si bonding of this partially charged Si. On further attack by the additional OH^-; a soluble silicate[26] forms to complete a Si atom etching process and two more electrons are liberated. Consequently, four electrons are liberated during a complete Si etching reaction, and two H_2 are generated by the reduction of H_2O as indicated in Eq. 1. This kind of simultaneous reduction-oxidation at a single spot is often encountered. For example, a pitting corrosion occurs for stainless steel in NaCl solution where the active site suffers anodic corrosion while the surrounding area acts as a cathodic reaction site.[27]

Etch stop mechanism in heavily doped silicon.—Although the technique of etch stop in heavily doped Si is widely used in device manufacturing, the mechanism of the etch stop is still not clear. Palik *et al.*[11] attribute the reduction of the etching rate in heavily doped Si to the formation of an oxide film. From ellipsometric measurements, a spontaneously formed oxide film was found in the p-Si with the boron doping concentration greater than $1 \times 10^{19}/cm^3$ and a prepassive layer was found in heavily phosphorus-doped n-Si. Raley *et al.*[23] found that the etch rate decrease is sensitive to hole concentration and not sensitive to atomic concentration of boron or strain. They attributed this etch rate decrease to the diminished number of electrons through

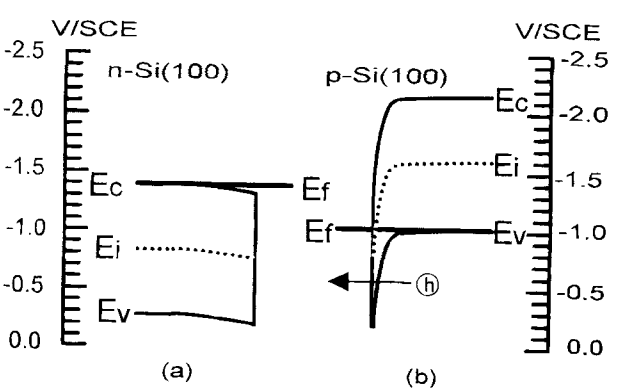

Fig. 11. The energy band diagrams of heavily doped (a) n-Si and (b) p-Si.

Auger recombination with holes. The lack of electrons stops the reduction reaction and interrupts the reduction-oxidation cycle. Seidel *et al.*[28] agree with this hole-interrupt model, and expect that etching to occur for heavily doped n-Si.

In this article, the etch stop mechanism in heavily doped Si is attributed to the enhancement of the oxide film growth rate under high carrier concentration. This mechanism is consistent with all experimental observations just described including the formation of an oxide film, and the role of high carrier concentration. The band diagrams of heavily doped n-Si and p-Si in contact with the KOH electrolyte before the formation of an oxide film are illustrated in Fig. 11a and b, respectively. The OCP measured for $5 \times 10^{20}/cm^3$ phosphorus-doped n-Si is -1.36 V and $2.8 \times 10^{20}/cm^3$ boron-doped p-Si is -1.00 V.[16] The built-in potential for $5 \times 10^{20}/cm^3$ n-Si is reduced to 0.05 eV (about $2kT$). Holes in the bulk Si can easily be thermally excited and emitted to the Si/KOH interface. These thermo-emitted holes can participate in the oxidation reaction and form an oxide film. Due to the limited number of holes, which are minority carriers in the n-Si, the oxidation rate is restricted and an incomplete prepassive film is formed as observed by Palik *et al.*[11] As for the heavily doped p-Si, the thickness of the depletion layer decreases to a few angstroms and the hole can tunnel through the barrier freely to the Si surface. Since a dense oxide film is formed with the assistance of these holes, the etch rate drops abruptly.

Conclusion

The energy band diagram of n-Si in 2*M* KOH was constructed by measuring the OCP and the flatband voltage. The flatband voltage of n-Si in KOH is -1.04 V which was determined by photocurrent susceptivity method. The energy band diagram of p-Si was constructed according to the assumption of equal electron affinity for both n-Si and p-Si in KOH. At equilibrium, the energy band bends downward near the interface for both n- and p-Si. For the n-Si, there exists an accumulation layer at the interface. While for p-Si, there exists a potential barrier and a depletion region near the interface. This leads to an ohmic-contact-like I-V characteristic for n-Si, and a Schottky-contact-like I-V characteristic for p-Si. Before the passivation peak, a linear I-V relation for n-Si and a rectifying characteristic for p-Si were observed. These characteristics are consistent with the energy band diagrams for Si in aqueous KOH. When applying an anodic bias greater than PP, the structure changes from Si/electrolyte to Si/oxide/electrolyte. The anodic currents of n-Si and p-Si are attributed to the electrochemical formation of the oxide film. Holes in the inversion layer of the n-Si and in the accumulation layer of the p-Si contribute to the oxide film formation. The formation of these holes can be explained clearly with the aid of energy band diagrams. The effect of illumination on OCP and on I-V curves of n-Si and p-Si also can be understood through the energy band model. The etching mechanisms as well as the carrier-transport phenomena of Si in KOH can be explained with the aid of energy band diagrams. The competition between the oxidation rate and the diffusion rate of oxidation product determines whether the anodic oxidation is an etching or passivation process. The etchstop mechanism in heavily doped Si is attributed to the enhancement of the oxide film growth rate at high carrier concentrations.

Manuscript submitted June 6, 1994; revised manuscript received Aug. 24, 1994.

National Tsing Hua University assisted in meeting the publication costs of this article.

LIST OF SYMBOLS

OCP	open-circuit potential
PP	passivation potential
χ	electron affinity
E_{cs}	bottom of the conduction band at interface
E_c	bottom of the conduction band
E_f	Fermi level
E_i	intrinsic Fermi level
E_v	top of the valence band
$q\Phi_f$	$E_c - E_f$
V_c	cathodic bias
V_a	anodic bias
V_{FB}	flatband voltage
ϕ_f	Fermi potential
ϕ_s	built-in potential

REFERENCES

1. Y. P. Xu and R. S. Huang, *This Journal,* **137,** 948 (1990).
2. P. Bindra, H. Gerischer, and D. M. Kolb, *ibid.,* **124,** 1012 (1977).
3. A. J. Bard and M. S. Wrighton, *ibid.,* **124,** 1706 (1977).
4. H. Gerischer, *J. Vac. Sci. Technol.,* **15,** 1422 (1978).
5. G. Stremsdoerfer, H. Perrot, J. R. Martin, and P. Clechet, *This Journal,* **135,** 2881 (1988).
6. M. Hirata, S. Suwazono, and H. Tanigawa, *ibid.,* **134,** 2037 (1987).
7. E. D. Palik, O. J. Glembocki, and R. E. Stahlbush, *ibid.,* **135,** 3126 (1988).
8. B. Kloeck, S. D. Collins, N. F. De Rooij, and R. L. Smith, *IEEE Trans. Electron Devices,* **ED-36,** 663 (1989).
9. P. M. Sarro and A. W. van Herwaarden, *This Journal,* **133,** 1724 (1986).
10. Elie S. Ammar and T. J. Rodgers, *IEEE Trans. Electron Devices,* **ED-27,** 907 (1980).
11. E. D. Palik, V. M. Bermudez, and O. J. Glembocki, *This Journal,* **132,** 135 (1985).
12. E. D. Palik, O. J. Glembocki, and I. Heard, Jr., *ibid.,* **134,** 404 (1987).
13. C. H. Ozdemir and J. G. Smith, *Sensors and Actuators,* **A34,** 87 (1992).
14. H. Seidel, L. Csepregi, A. Heuberger, and H. Baumgartel, *This Journal,* **137,** 3612 (1990).
15. K. B. Sundaram and H. W. Chang, *ibid.,* **140,** 1592 (1993).
16. E. D. Palik, J. W. Faust, Jr., H. F. Gray, and R. F. Greene, *ibid.,* **129,** 2051 (1982).
17. O. J. Glembocki and R. E. Stahlbush, *ibid.,* **132,** 145 (1985).
18. P. Allongue, V. Costa-Kieling, and H. Gerischer, *ibid.,* **140,** 1009 (1993).
19. S. R. Morrison, *Electrochemistry at Semiconductor and Oxidized Metal Electrodes,* p. 64, Plenum Press, New York (1980).
20. W. H. Brattain and C. G. B. Garrett, *Bell Syst. Tel. J.,* **34,** 129 (1955).
21. J. W. Faust, Jr. and E. D. Palik, *This Journal,* **130,** 1413 (1983).
22. E. D. Palik, V. M. Bermudez, and O. J. Glembocki, *ibid.,* **132,** 871 (1985).
23. N. F. Raley, Y. Sugiyama, and T. Van Duzer, *ibid.,* **131,** 161 (1984).
24. L. Smith and A. Soderbarg, *ibid.,* **140,** 271 (1993).
25. P. Allongue, V. Costa-Kieling, and H. Gerischer, *ibid.,* **140,** 1018 (1993).
26. E. D. Palik, H. F. Gray, and P. B. Klein, *ibid.,* **130,** 956 (1983).
27. M. G. Fontana, *Corrosion Engineering,* 3rd ed., p. 63, McGraw-Hill, New York (1986).
28. H. Seidel, L. Csepregi, A. Heuberger, and H. Baumgartel, *This Journal,* **137,** 3626 (1990).